# Characterization of alginate-capped nanosilver by fractal and entropy analysis on its transmission electron microphotographs

Atharva Damle [a],[1], Sangeetha Muthusamy [a],[1], Reetoja Nag [b],[1], Raunak Kumar Das [b], Priyanka Srivastava [a],*

[a] Department of Biosciences, School of Bio Sciences and Technology, Vellore Institute of Technology, Vellore , Tamil Nadu, 632014, India
[b] Centre for Biomaterials, Cellular and Molecular Theranostics, Vellore Institute of Technology, Vellore, Tamil Nadu, 632014, India

## ARTICLE INFO

## ABSTRACT

The study employs conventional techniques and quantitative image analysis tools to characterize alginate-capped nanosilver synthesized by green methods. Sodium Alginate (0.5 %, 1 % and 2 %) was used as a reducing and stabilizing agent. Presence of particles was confirmed by UV–vis Spectroscopy, with absorbance maxima of 412−413 nm for 0.5 %, 1 % and 2 % of polymer. Hydrodynamic sizes of particles recorded for 0.5 %, 1 % and 2 % polymer were 128.4 ± 1.5, 129.9 ± 3.6 and 148.6 ± 1.0 nm by DLS. TEM revealed roughly spherical to cuboidal particles ranging from 15−20 nm and clusters of 100 nm and Energy Dispersive X-ray Spectroscopy confirmed the presence of silver in the particles. Analysis of the TEM images was done in MATLAB R2016b using histogram equalisation for image enhancement and entropy filtering for image segmentation. These techniques revealed the surface pores and polymer distribution around the particle. Statistical analysis (ANOVA) was performed for the measured fractal dimensions of nanoparticles with polymer coating, width of particle together with polymer coating, and thickness of only polymer coating around the particle for various study groups. Significant differences ($p < 0.05$) were found both between and within the study groups for fractal dimensions of nanoparticles with polymer coating, width of nanoparticles and thickness of polymer coating alone. The analysis was successful in confirming presence and thickness of polymer layer on particles.

## 1. Introduction

Nanobiotechnology offers multidisciplinary applications. The unique properties of the nanoparticles, including their high surface area to volume ratio, have found use in wide range of applications (Navya and Daima, 2016; Petros and DeSimone, 2010). Two main approaches for synthesis of nanoparticles are chemical and physical synthesis. High yield of nanoparticles is achieved from both approaches, but they have their share of disadvantages (Abou El-Nour et al., 2010). They are costlier, energy consuming, particularly controlling particle size and distribution is difficult in physical methods of synthesis, whereas production of toxic by-products are a challenge in chemical synthesis methods (Tavakoli et al., 2007). These disadvantages lead to evolution of green synthesis approaches. The green synthesis approaches include synthesis from microbial, plant or algal cells or their derivatives. These approaches have several advantages over chemical and physical

synthesis methods like being environmentally safe, produce less toxic by-products, have high biocompatibility, higher productivity, economic viability and ease of handling or manipulation (Gudikandula and Maringanti, 2016).

Silver nanoparticles (AgNPs) are popularly used in biomedical field, pharmaceutical industry and food packaging industry due to their antibacterial and physicochemical properties (Abou El-Nour et al., 2010; Sharma et al., 2012). The silver nanoparticles exhibit very potent antimicrobial action due to their large surface area and their ability to reserve and release $Ag^+$ ions. Moreover, this antimicrobial activity has been reported against both Gram positive and Gram negative bacteria (Dallas et al., 2011). This regulated $Ag^+$ release mechanism depends on the morphological characteristics and assures the antibacterial endurance (Shao et al., 2018). The microbial synthesis of nanoparticles is largely affected by pH, temperature and microbial growth conditions and its purification requires an additional step of downstream
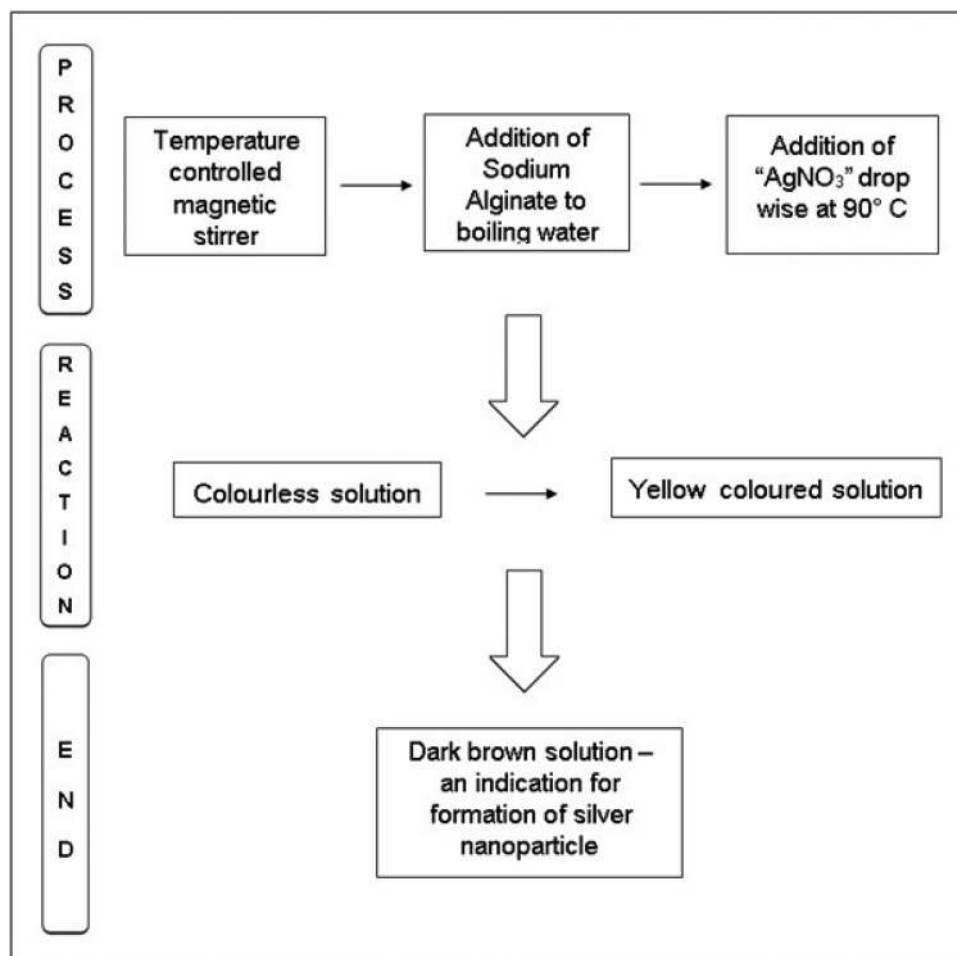
---

**Fig. 1.** Schematic diagram for the synthesis of Ag/SA nanobiocomposites.

processing (Thakkar et al., 2010; Iravani, 2014). The syntheses of nanoparticles from plant and microbial extracts also have a few disadvantages. Most of the compounds in plants responsible for reduction of metal salt to nanoparticles are secondary metabolites and as such, their production varies with various environmental fluxes. Moreover, using extract rather than a known purified compound offers little control as far as tunability in synthesis is concerned (Ahmed et al., 2016). Hence, the synthesis of nanoparticles is not reliable and reproducible. To overcome this disadvantage in phyto- and microbial synthesis approaches, the present study focuses on combining biopolymers derived from natural sources and AgNPs.

Biopolymers were earlier used in synthesis of nanoparticles leading to the birth of bio-nanocomposites (Arora et al., 2018). In the present study, a naturally occurring polysaccharide Sodium Alginate (SA) was used as a reductant as well as a stabiliser. It is a hydrophilic anionic polymer extracted from marine brown algae of the Phaeophyceae family. It is widely used in the food and pharmaceutical industry. It is a binary copolymer of $1 \rightarrow 4$ linearly linked chains of β-D-mannuronic acid and α-L-guluronic acid. It can serve as a colloidal reducer and stabiliser in green synthesis of silver nanocomposites due to its biocompatibility, availability, low production cost, non-toxicity and presence of many functional groups (Sharma et al., 2012; Yang et al., 2014).The advantages of both silver and alginate were combined to synthesise Ag/SA nanocomposites. These composite nanostructures have a wide application in the biomedical field. They are employed for inhibiting wound infection, wound healing and can also be used for the disruption and inhibition of biofilms on prosthetics or biomedical devices (Pei et al.,

2015; Scholz et al., 2011). The polymer surface can be impregnated with antibiotics for a regulated drug release and to get a synergistic antimicrobial effect with silver (Velusamy et al., 2016).

Transmission Electron Microscopy (TEM) imaging is a powerful and traditional characterization technique. The resulting images can be analysed by quantitative image analysis, as this technique amplifies the data which is not revealed due to the limitations of electron microscopy. Quantitative image analysis is widely used in fields like metal industry and medical field to identify mechanical imperfections of products during processing and to assess the conduct and drug effectiveness respectively (Eremin, 2006; Sahani et al., 2000; Pathak et al., 2003). The use of quantitative image analysis in a pharmaceutical production environment has been depicted in literature by only a few papers in spite of its usefulness (Ho et al., 2007; Wu et al., 2007; Zeitler et al., 2007; Ho et al., 2008; Spencer et al., 2008). Earlier, terahertz pulsed imaging technique has been used to calculate and quantify coating thickness of tablets, where the coating included the pore constitution (Laksmana et al., 2009). Previously, for images of coated particles obtained with Confocal Laser Scanning Microscopy, the coating thickness and particle perimeter were determined using image analysis tools in MATLAB. The methodology used helped in providing a realistic and logical design to develop a characterization method for coated particles used in the pharmaceutical industry (Laksmana et al., 2009).

Therefore, the focus of the present study is compare conventional characterization methods with characterization using quantitative image analysis, of the synthesized bionanocomposites, to figure out new information that could be obtained from latter.

## 2. Materials and methods

Alginic acid sodium salt from brown algae (Sodium Alginate) of Sigma Life Sciences and Silver Nitrate ($AgNO_3$) of HiMedia BioSciences was used for synthesis of silver nanobiocomposites. All chemicals were used without any further treatment or purification. Distilled water was used as a solvent in the experiment. A Temperature-Controlled Magnetic Stirrer (REMI 5 MLH PLUS) was used for synthesis. The experiments were performed in triplicates to optimize the findings.

### 2.1. Synthesis of silver nanocomposites

Silver nanobiocomposites were prepared by the reduction of $AgNO_3$ by Sodium Alginate (SA). 0.5 % (low), 1 % (medium) and 2 % (high) of SA were the different concentrations used for synthesis of silver nanocomposites. An aqueous solution of the respective SA concentrations was prepared and placed on Temperature- Controlled Magnetic Stirrer. A clear solution of freshly prepared 0.04 M $AgNO_3$ solution was prepared and added drop wise to the alginate solution, which was maintained at 90 °C. Temperature is very crucial in the synthesis and hence, the reaction temperature was maintained at 90 °C throughout the experiment (Sharma et al., 2012). The total volume ratio of SA salt and $AgNO_3$ was 4:1 respectively (Fig. 1). The reaction time varied according to concentration of SA and 0.5 %, 1 % and 2 % SA took 50, 30 and 25 min respectively, for the reaction to complete. The colloidal solution underwent colour changes from transparent to yellow to dark brown during the reaction process. The dark brown colour denoted the endpoint of the reaction, indicating the synthesis of nanoparticles. The synthesized silver colloidal solution was stored in glass scintillation vials, wrapped with aluminium foil, and kept in dark protected from light, at room temperature.

### 2.2. Characterisation

#### 2.2.1. UV–vis spectroscopy

The presence of the sliver nanobiocomposites was confirmed by UV–vis Spectrophotometry (HITACHI U-2800 Spectrophotometer). Baseline correction of spectrophotometer was done using the reference as distilled water. The samples were diluted with distilled water. The dilution factor for each sample was 5 i.e. 800 μL: 3200 μL (sample:water) for all concentrations. The samples were scanned in the range of 200−900 nm.

#### 2.2.2. Dynamic light scattering (DLS) and zeta analysis

The hydrodynamic size and stability of the nanoparticles was evaluated using Dynamic Light Scattering (Nanoparticle Analyser HORIBA Scientific SZ-100). The charge on the synthesized nanoparticles and the dispersion of the nanoparticles in the medium was interpreted by Zeta Potential Analysis and its Polydispersity Index. The temperature and detector setting in the sample cell was set up at 25 °C and detection angle (stationary) of 90°. The same dilution factor of 5 was taken for the analysis.

#### 2.2.3. Transmission Electron Microscopy (TEM) & energy dispersive X-ray (EDX) spectroscopy

Transmission Electron Microscope (FEI TECNAI G2-20 TWIN) was used to determine the size and morphology of silver nanoparticles. The sample preparation is an important aspect in TEM analysis. The samples were diluted with distilled water to achieve optimum concentration for their analysis. Then the particles were dispersed by sonicating for 10−15 min in a water-bath sonicator. A drop of sonicated sample was taken and casted on carbon-coated copper grid. The samples were allowed to dry to form a small thin disk. These samples were imaged at an accelerating voltage 200 kV under different magnifications.

Energy Dispersive X-ray (EDX) analysis (BRUKER) confirmed the elemental composition of the nanoparticles.

### 2.3. Image analysis

The image analysis was performed using the image processing toolbox provided in MATLAB R2016b. The images with different concentrations of polymer (0.5 %, 1 % and 2 %) on the nanoparticle were first enhanced using contrast enhancement using Histogram Equalization (HISTEQ) command in MATLAB image processing toolbox and segmented using entropy texture segmentation method. Texture analysis is the characterisation of regions in an image by their texture content i.e. roughness which in turn refers to variations in pixel intensity values. High entropy is associated with a high variance in the pixel values, while low entropy indicates that the pixel values are fairly uniform (Mole and Ganesan, 2011). When applied to groups of pixels within the images, entropy provides a way to evaluate regions within the images. For entropy calculation, for each pixel p = (u, v) in the final image, corresponding pixels p1, p2, …, pN is considered in the original image. Every pixel in the final image is computed as the weighted average of the corresponding pixels in the original image (German et al., 2005). The entropy of a pixel $v_i$ and the weighted average $p$ are given by Eq. (1) and Eq. (2) respectively, where $q_i$ is the probability that a random pixel $p_i$ chosen will have intensity i,

$$v_i = \sum_k - q_k \, X \log 2( q_k ) \tag{1}$$

$$p = \sum_{i=1}^{N} (p_i v_i) / \sum_{i=1}^{N} (v_i) \tag{2}$$

### 2.4. Quantification

The quantification comprised the determination of the width and fractal dimension of the nanoparticle including the polymer coating and the thickness of the polymer coating alone. The width of the nanoparticles along with polymer coating and the thickness of the polymer coating were calculated using distance tool and distance equation function in MATLAB 2016b software. Irregular geometric figures, which do not follow the rules of regular Euclidean geometry, and are characterized by self-similarity property are called as fractals (Ga, 1995; Avnir et al., 1998). The assessment and quantification of the degree of complexity and irregularity of these objects gives measurements called "fractal dimensions'' (FD) (Goutzanis et al., 2008). The most widely used method of estimation of the fractal dimension is the box-counting algorithm used by several computer programs. In this algorithm, FD is more specifically termed as the box-counting dimension (DB) (Delides et al., 2005; Li et al., 2009). The FD of the nanoparticles along with polymer coating was calculated using the box counting algorithm in MATLAB R2016b software.

### 2.5. Statistical analysis

50 values each for the width of the nanoparticles along with polymer coating, fractal dimension of the nanoparticles along with polymer coating and thickness of the polymer coating alone was calculated for all the different concentrations of the polymer coating i.e. (0.5 %, 1 % and 2 %). All the values were measured in pixels. The values were then statistically analysed using ANOVA test to find out the significant differences between and within the 3 different study groups i.e. nanoparticle with polymer coating with different concentrations (0.5 %, 1 % and 2 %).

## 3. Results and discussion

### 3.1. UV–vis spectroscopy

The metallic nanoparticles show a unique property restricted to metals called surface plasmon resonance. Due to this property different metallic nanoparticles have a unique absorbance maximum. Although a
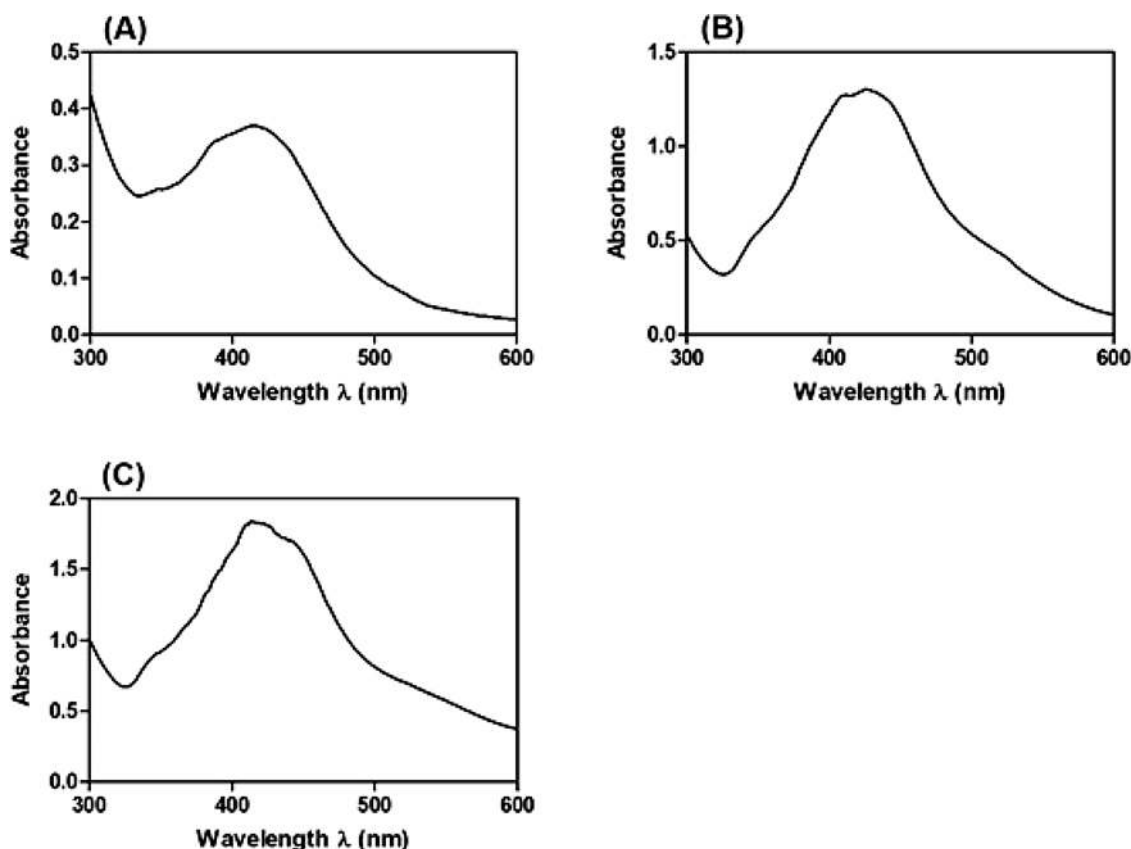
**Fig. 2.** UV–vis spectra demonstrating formation of silver nanoparticles at different polymer concentrations (A) 0.5 % (B) 1 % (C) 2 %.

simple technique, UV–vis Spectroscopy becomes a powerful and important technique for confirming the presence of metallic nanoparticles. The absorbance maxima of nanoparticles were found to be 413 nm, 412 nm and 413 nm for concentrations of 0.5 %, 1 % and 2 %, respectively (Fig. 2). These characteristic absorbance maxima confirmed the presence of silver nanoparticles in the colloidal solution.

### 3.2. Dynamic light scattering (DLS) and zeta analysis

The hydrodynamic size of the nanoparticles was recorded by Dynamic Light Scattering (DLS) study of the nanoparticles. The particles in Brownian motion have a varying scattering with respect to their hydrodynamic size. The hydrodynamic size includes the layer of solvent molecules on the nanoparticle surface along with the actual diameter of the particle. The hydrodynamic sizes were found to be $128.36 \pm 1.46$ nm, $129.9 \pm 3.6$ nm, $148.6 \pm 1$ nm for the concentrations of 0.5 %, 1 % and 2 % respectively (Table 1). Though DLS is mostly used to confirm size distribution of nanoparticles, characterisation of long term stability in different media as well as their pH values and aggregation profile identification have also been used by DLS technique (Mohanty et al., 2013; Casciaro et al., 2017; Zhang et al., 2018).

**Table 1**
Average hydrodynamic sizes of the nanoparticles for the corresponding polymer concentration.

| S. No. | Sodium Alginate (%) | Hydrodynamic Size (nm) | Polydispersity Index (PDI) | Zeta Potential (mV) |
|---|---|---|---|---|
| 1. | 0.5 % | $128.36 \pm 1.46$ | 0.345 | 0.1 |
| 2. | 1 % | $129.9 \pm 3.6$ | 0.221 | 0.0 |
| 3. | 2 % | $148.6 \pm 1$ | 0.552 | 1.8 |

Some of the areas where zeta potential can be used, are optimization of peptide-anchoring profile to the nanoparticle, confirmation of surface charge modification, and validation of electrostatic interaction between the nanoparticle and the target cells, etc. (Kuai et al., 2010; Takara et al., 2010; Pal et al., 2016). The Zetasizer studies were not relevant as a polymer was used as a stabiliser for the synthesis of the nanoparticles. The nanoparticles were well dispersed and sterically stable in the colloidal mixture. Hence, stability by steric hindrance was given more importance than the stability by charge as a parameter.

### 3.3. Transmission Electron microscopy (TEM) and energy dispersive X-ray spectroscopy (EDX)

The TEM images of nanoparticles at all three concentrations of Sodium Alginate were studied. Predominantly, nanoparticles exhibited a spherical morphology. Preliminary analysis of raw images indicated that most nanoparticles had a diameter of approximately 20 nm at a polymer concentration of 0.5 %. The nanoparticles at a polymer concentration of 1 % had a diameter of approximately 15 nm. At both concentrations, nanoparticles were well dispersed in the medium. Large clusters were observed at a polymer concentration of 2 %. Due to the higher polymer concentration, the nanoparticles were agglomerated. Smaller spherical nanoparticles were seen attached to larger cuboidal nanoparticles with a size of approximately 100 nm. The images indicated initiation of formation of nanocubes from 'nucleation' by smaller silver particles. The formation of such cubes is dependent on the capping polymer, reaction temperature, reactant concentration, reaction time and reactant molar ratios (Wiley et al., 2005; Tao et al., 2006; Khodashenas and Ghorbani, 2019). These images were further analysed by computerized quantitative image processing to extract further statistical data.

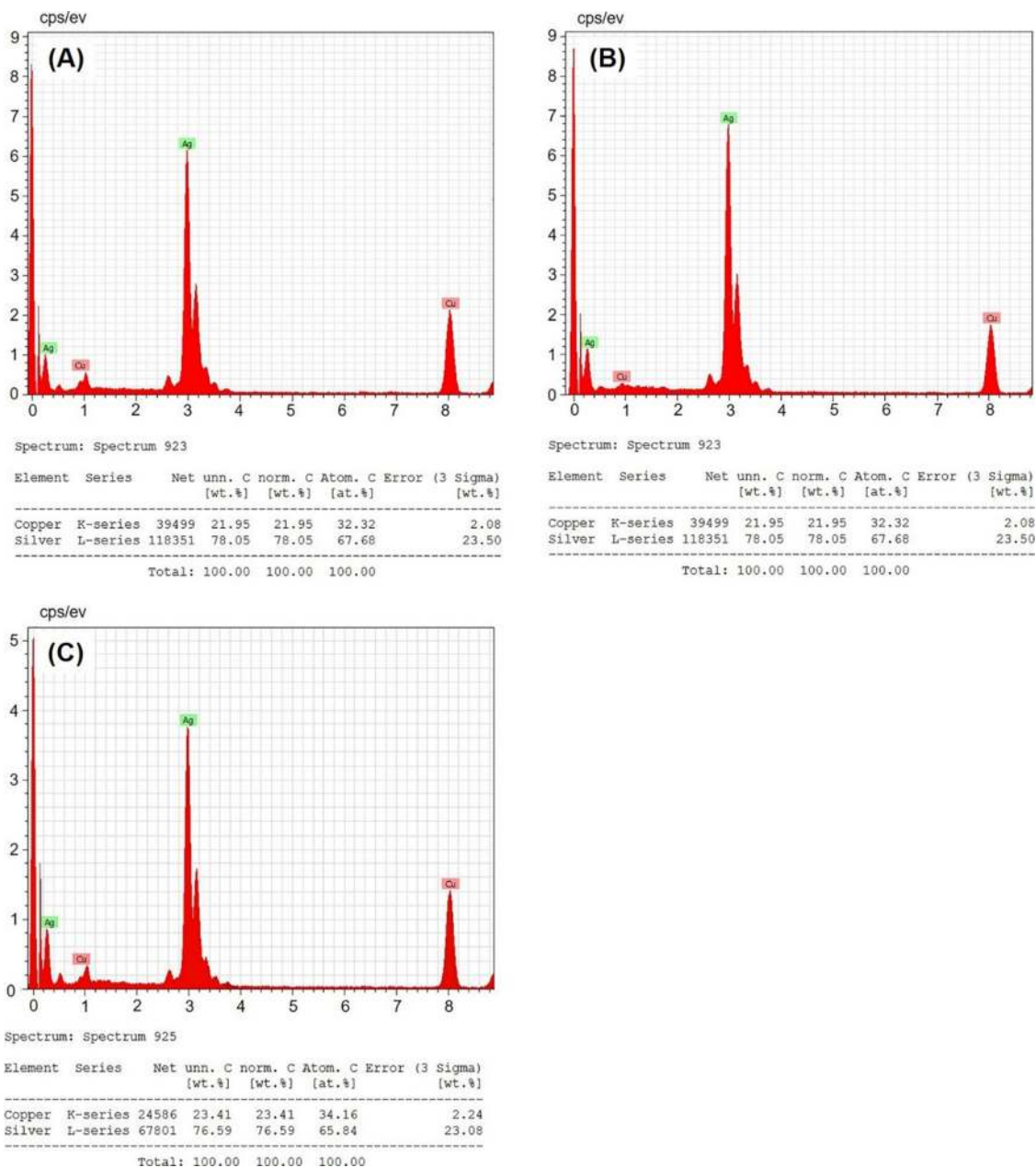Energy Dispersive X-ray Spectroscopy (EDX) results confirmed that

**Fig. 3.** EDX analysis for confirmation of presence of silver in particles. Peak for copper is due to the copper grids on which the particles were imaged.
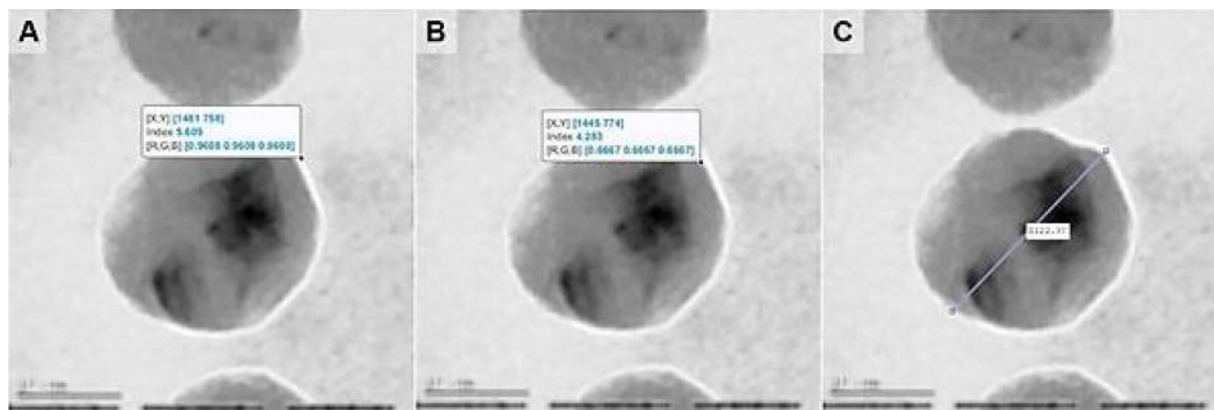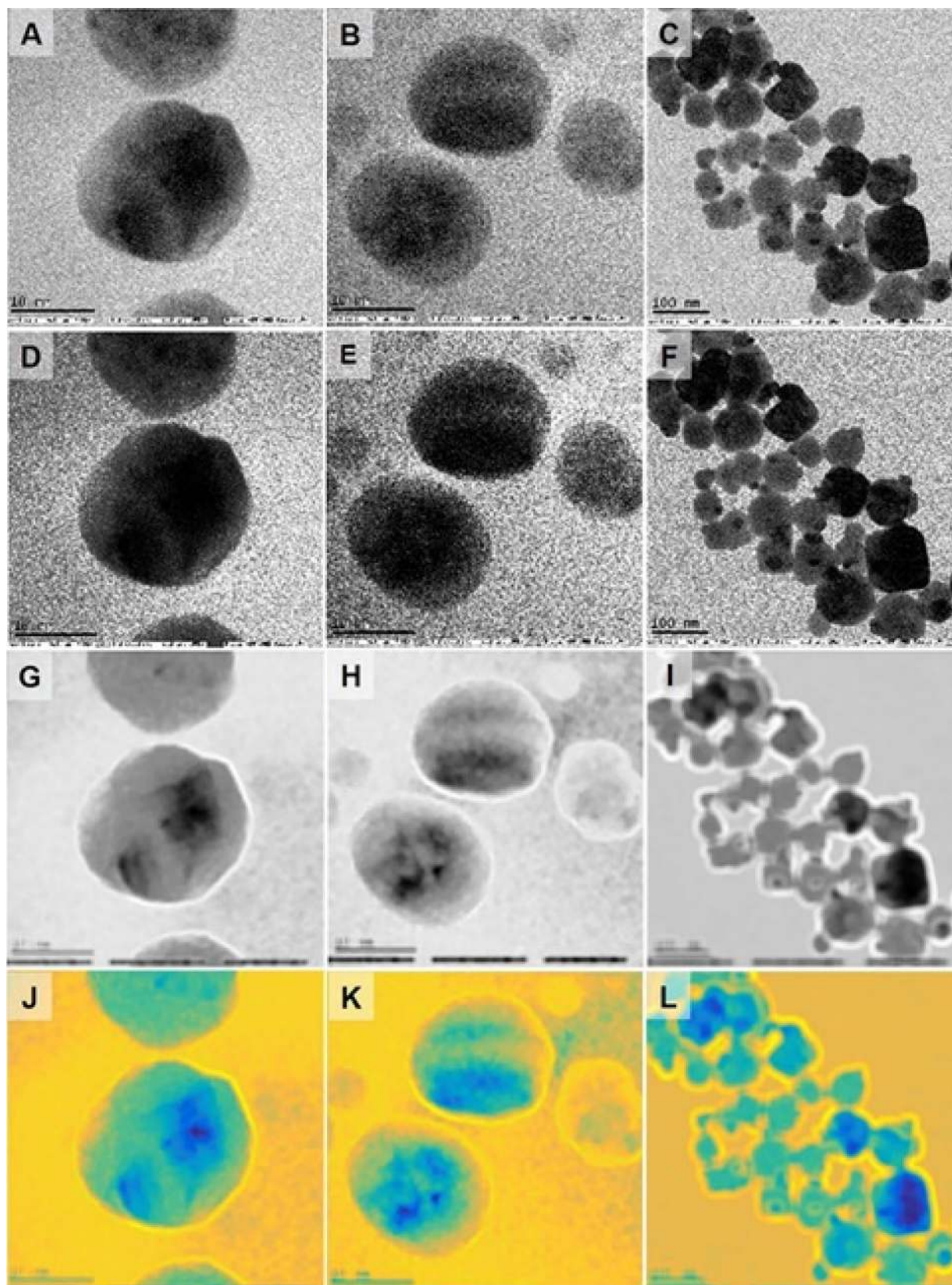


**Fig. 4.** (A) Example of thickness of polymer layer (B) Example of thickness of polymer-1 coordinate point (C) Example of calculation of distance of nanoparticle plus polymer.

**Fig. 5.** (A) Nanoparticle with 0.5 % concentration of polymer coating (B) Nanoparticle with 1 % concentration of polymer coating (C) Nanoparticle with 2 % concentration of polymer coating (D) Histogram equalisation on nanoparticle with 0.5 % concentration of polymer coating (E) Histogram equalisation on nano-particle with 1 % concentration of polymer coating (F) Histogram equalisation on nanoparticle with 2 % concentration of polymer coating (G) Entropy filter on nanoparticle with 0.5 % concentration of polymer coating (H) Entropy filter on nanoparticle with 1 % concentration of polymer coating (I) Entropy filter on nanoparticle with 2 % concentration of polymer coating (J) False colormap of (G); (K) False colormap of (H); (L) False colormap of (I).

**Table 2**

ANOVA test for determining the statistical significance between and within the study groups (0.5 %, 1 % and 2 % concentration of polymer coating on nanoparticle) for attributes of the nanoparticle with polymer coating.

| Attribute | 0.5 % polymer coating on nanoparticle | 1 % polymer coating on nanoparticle | 2 % polymer coating on nanoparticle | *p*-values between the study groups | ANOVA Test | *p*-values within the study groups |
|---|---|---|---|---|---|---|
| Width of nanoparticle with polymer coating | 130.8036 + 38.5251 | 154.0138 + 60.5363 | 214.9408 + 56.0641 | <0.00001 | 0.5 % vs. 1 % | 0.024 |
| | | | | | 1 % vs. 2 % | <0.00001 |
| | | | | | 0.5 % vs. 2 % | <0.00001 |
| Fractal Dimension of nanoparticle with polymer coating | 1.8637+0.0808 | 1.8495 + 0.086 | 1.8066 + 0.0903 | 0.003 | 0.5 % vs. 1 % | 0.396 |
| | | | | | 1 % vs. 2 % | 0.016 |
| | | | | | 0.5 % vs. 2 % | 0.001 |
| Thickness of polymer coating | 39.8648 + 10.8649 | 43.9771 + 8.6644 | 57.541 + 9.338 | <0.00001 | 0.5 % vs. 1 % | 0.038978 |
| | | | | | 1 % vs. 2 % | <0.00001 |
| | | | | | 0.5 % vs. 2 % | <0.00001 |

the particles consisted of Silver (Ag). The graph also showed a peak for Carbon (unlabelled peak at 0.1 eV) and Copper (Cu), as a Carbon coated Copper grid was used for sample analysis (Fig. 3). EDX data acquisition is comparatively newer than other imaging modalities like Electron Energy Loss Spectroscopy (EELS). It has an advantage of determination of small amounts of heavy elements in fairly large nanoparticles, whereas EELS has higher detection sensitivity for light elements. (Müllejans and Bruley, 1993; Slater et al., 2016)

*3.4. Image analysis*

The polymer coating of nanoparticles for different concentrations of the polymer (0.5 %, 1 % and 2 %) are clearly shown in Figs. 4(A), 3 (B) and (C) respectively. The original images of the nanoparticles with polymer coating with concentrations 0.5 %, 1 % and 2 % are shown in Fig. 5(A), (B) and (C) respectively. The histogram equalised results for Fig. 5(A), (B) and (C) are shown in Figs. 5(D), 4 (E) and (F) respectively. The segmentation by entropy filter to show the coating of polymer on the nanoparticles done on Fig. 5(D), (E) and (F) are shown in Figs. 5(G), 4 (H) and (I) respectively. The false colormap of the Fig. 5(G), (H) and (I) are shown in Fig. 5(J), (K) and (L) respectively.

The results of the ANOVA test to determine statistically significant differences ($p < 0.05$) both within and between the study groups (i.e. 0.5 % polymer coating on nanoparticle, 1 % polymer coating on nanoparticle and 2 % polymer coating on nanoparticle) for different attributes of the polymer coated nanoparticles (i.e. width of nanoparticle with polymer coating, fractal dimension of nanoparticle with polymer coating and thickness of the polymer coating), are given in Table 2. For width of the nanoparticles along with polymer coating, statistical significant difference was found between the study groups ($p < 0.00001$) as well as within all the study groups i.e. 0.5 % polymer coating on nanoparticles vs. 1 % polymer coating on nanoparticles ($p = 0.024$), 1 % polymer coating on nanoparticles vs. 2 % polymer coating on nanoparticles ($p < 0.00001$) and 0.5 % polymer coating on nanoparticles vs. 2 % polymer coating on nanoparticles ($p < 0.00001$). For fractal dimension of the nanoparticles along with polymer coating, statistical significant difference was found between the study groups ($p = 0.003$) as well as within the study groups i.e. 1 % polymer coating on nanoparticles vs. 2 % polymer coating on nanoparticles ($p = 0.016$) and 0.5 % polymer coating on nanoparticles vs. 2 % polymer coating on nanoparticles ($p = 0.001$). For thickness of polymer coating only, statistical significant difference was found between the study groups ($p < 0.00001$) as well as within all the study groups i.e. 0.5 % polymer coating vs. 1 % polymer

coating ($p = 0.038978$), 1 % polymer coating vs. 2 % polymer coating ($p < 0.00001$) and 0.5 % polymer coating vs. 2 % polymer coating ($p < 0.00001$).

Textures in images can be random or regularly structured hence, for segmentation, different texture-based image segmentation methods have been used. Previously, for texture-based image segmentation, methods such as Fourier transform, Gabor, Thresholding, Histogram and wavelet transforms have been used (Bhosle and Pawar, 2013).

Also, local spectral histograms were used to localise region boundaries and differentiate between region appearances thus effectively segmenting images based on texture (Yuan et al., 2015). Supervised texture segmentation was done using Markovian and Gaussian Mixture Texture models, which proved faster than unsupervised Markov Segmentation (Haindl and Mikes, 2008). Though many texture-based image segmentation methods have been used till date, most of them have been complex to compute, th, newer and simpler methods are much needed (Zaitoun and Aqel, 2015).

It has been shown that using the entropy filter-based texture segmentation method after contrast enhancement using histogram equalisation, the polymer coating of different concentrations (0.5 %, 1 % and 2 %) on the nanoparticle can be easily detected and visualised. To the best of our knowledge, use of entropy filter by image analysis has not been used previously to detect polymer coating on nanoparticle.

After statistical analysis (ANOVA) between the study groups (0.5 % concentration of polymer coating on nanoparticle, 1 % concentration of polymer coating on nanoparticle and 2 % concentration of polymer coating on nanoparticle), we found that there is statistical significant difference both between and within the study groups for the attributes width of nanoparticles with polymer coating and thickness of polymer coating alone. Hence, we can say that these two attributes have variation for different concentrations of polymer coating (0.5 %, 1 % and 2 %). For fractal dimension of the nanoparticles with polymer coating, except for 0.5 % polymer coating on nanoparticles vs. 1 % polymer coating on nanoparticles ($p = 0.396$), statistical significant difference was found both within and between the study groups, hence this attribute, with the exception of 0.5 % polymer coating on nanoparticles vs. 1 % polymer coating on nanoparticles, has variation for different concentrations of polymer coating.

**4. Conclusions**

The current study demonstrated characterization of synthesized nanobiocomposites by conventional techniques and image analysis.

Primarily, the TEM images were subjected to quantitative image analysis which aided in segmentation and visualisation of the nanoparticles with polymer coating of different concentrations. Since image analysis tools are quick and inexpensive they can be effective in characterizing nanoparticles in comparison to conventional procedures which are tedious and time taking. Additionally, the analysis also conveys the thickness of polymer layer which is important in applications of Surface Enhanced Raman Spectroscopy based imaging systems and drug delivery.

## Authors' contributions

AD, SM did the particle synthesis and characterizations. RN did the quantitative image analysis. RKD and PS developed the idea, monitored students work, helped in data analysis and manuscript writing.

## Funding

## Declaration of Competing Interest

Authors declare no conflict of interest.

## Acknowledgements

## References

Abou El-Nour, K.M.M., Eftaiha, A., Al-Warthan, A., Ammar, R.A.A., 2010. Synthesis and applications of silver nanoparticles. Arab. J. Chem. 3 (3), 135–140. https://doi.org/10.1016/j.arabjc.2010.04.008.

Ahmed, S., Ahmad, M., Swami, B.L., Ikram, S., 2016. A review on plants extract mediated synthesis of silver nanoparticles for antimicrobial applications: a green expertise. J. Adv. Res. 7 (1), 17–28. https://doi.org/10.1016/j.jare.2015.02.007.

Arora, B., Bhatia, R., Attri, P., 2018. 28 - Bionanocomposites: Green materials for a sustainable future. In: Hussain, C.M., Mishra, A.K. (Eds.), New Polymer Nanocomposites for Environmental Remediation. Elsevier, pp. 699–712. https://doi.org/10.1016/B978-0-12-811033-1.00027-5.

Avnir, D., Biham, O., Lidar, D.A., Malcai, O., 1998. Is the Geometry of Nature Fractal? Science. https://doi.org/10.1126/science.279.5347.39.

Bhosle, V.V., Pawar, V.P., 2013. Texture Segmentation: Different Methods, Vol. 3, p. 6 (5).

Casciaro, B., Moros, M., Rivera-Fernández, S., Bellelli, A., de la Fuente, J.M., Mangoni, M.L., 2017. Gold-nanoparticles coated with the antimicrobial peptide esculentin-1a (1-21) NH2 as a reliable strategy for antipseudomonal drugs. Acta Biomater. 47, 170–181. https://doi.org/10.1016/j.actbio.2016.09.041.

Dallas, P., Sharma, V.K., Zboril, R., 2011. Silver polymeric nanocomposites as advanced antimicrobial agents: classification, synthetic paths, applications, and perspectives. Adv. Colloid Interface Sci. 166 (1–2), 119–135. https://doi.org/10.1016/j.cis.2011.05.008.

Delides, A., Panayiotides, I., Alegakis, A., Kyroudi, A., Banis, C., Pavlaki, A., Helidonis, E., Kittas, C., 2005. Fractal dimension as a prognostic factor for laryngeal carcinoma. Anticancer Res. 25 (3B), 2141–2144.

Eremin, S.N., 2006. Image processing technology in the systems for quality control of sheet metal roll. Pattern Recognit. Image Anal. 16 (1), 127–130. https://doi.org/10.1134/S1054661806010408.

Ga, L., 1995. Fractals in pathology: are they really useful? Pathologica 87 (3), 310–317.

German, A., Jenkin, M.R., Lespérance, Y., 2005. Entropy-based image merging. In: The 2nd Canadian Conference on Computer and Robot Vision (CRV'05). IEEE, pp. 81–86. https://doi.org/10.1109/CRV.2005.38.

Goutzanis, L., Papadogeorgakis, N., Pavlopoulos, P.M., Katti, K., Petsinis, V., Plochoras, I., Pantelidaki, C., Kavantzas, N., Patsouris, E., Alexandridis, C., 2008. Nuclear fractal dimension as a prognostic factor in oral squamous cell carcinoma. Oral Oncol. 44 (4), 345–353. https://doi.org/10.1016/j.oraloncology.2007.04.005.

Gudikandula, K., Maringanti, S.C., 2016. Synthesis of silver nanoparticles by chemical and biological methods and their antimicrobial properties. J. Exp. Nanosci. 11 (9), 714–721. https://doi.org/10.1080/17458080.2016.1139196.

Haindl, M., Mikes, S., 2008. Unsupervised Texture Segmentation. Pattern Recognition Techniques, Technology and Applications. https://doi.org/10.5772/6243.

Ho, L., Müller, R., Römer, M., Gordon, K.C., Heinämäki, J., Kleinebudde, P., Pepper, M., Rades, T., Shen, Y.C., Strachan, C.J., Taday, P.F., Zeitler, J.A., 2007. Analysis of sustained-release tablet film coats using terahertz pulsed imaging. J. Control. Release 119 (3), 253–261. https://doi.org/10.1016/j.jconrel.2007.03.011.

Ho, L., Müller, R., Gordon, K.C., Kleinebudde, P., Pepper, M., Rades, T., Shen, Y.C., Taday, P.F., Zeitler, J.A., 2008. Applications of terahertz pulsed imaging to sustained-release tablet film coating quality assessment and dissolution performance. J. Control. Release 127 (1), 79–87. https://doi.org/10.1016/j.jconrel.2008.01.002.

Iravani, S., 2014. Bacteria in Nanoparticle Synthesis: Current Status and Future Prospects [Review Article]. International Scholarly Research Notices, Hindawi. https://doi.org/10.1155/2014/359316.

Khodashenas, B., Ghorbani, H.R., 2019. Synthesis of silver nanoparticles with different shapes. Arab. J. Chem. 12 (8), 1823–1838. https://doi.org/10.1016/j.arabjc.2014.12.014.

Kuai, R., Yuan, W., Qin, Y., Chen, H., Tang, J., Yuan, M., Zhang, Z., He, Q., 2010. Efficient delivery of payload into tumor cells in a controlled manner by TAT and thiolytic cleavable PEG co-modified liposomes. Mol. Pharm. 7 (5), 1816–1826. https://doi.org/10.1021/mp100171c.

Laksmana, F.L., Van Vliet, L.J., Hartman Kok, P.J.A., Vromans, H., Frijlink, H.W., Van der Voort Maarschalk, K., 2009. Quantitative image analysis for evaluating the coating thickness and pore distribution in coated small particles. Pharm. Res. 26 (4), 965–976. https://doi.org/10.1007/s11095-008-9805-y.

Li, J., Du, Q., Sun, C., 2009. An improved box-counting method for image fractal dimension estimation. Pattern Recognit. 42 (11), 2460–2469. https://doi.org/10.1016/j.patcog.2009.03.001.

Mohanty, S., Jena, P., Mehta, R., Pati, R., Banerjee, B., Patil, S., Sonawane, A., 2013. Cationic antimicrobial peptides and biogenic silver nanoparticles kill mycobacteria without eliciting DNA damage and cytotoxicity in mouse macrophages. Antimicrob. Agents Chemother. 57 (8), 3688–3698. https://doi.org/10.1128/AAC.02475-12.

Mole, S.S.S., Ganesan, L., 2011. Unsupervised texture classification of entropy based local descriptor using k-means clustering algorithm. Int. J. Comput. 10 (2), 133–140.

Müllejans, H., Bruley, J., 1993. Electron energy-loss spectroscopy (EELS); comparison with X-ray analysis. J. Phys. IV 03 (C7), C7–2083-C7-2092. https://doi.org/10.1051/jp4:19937332.

Navya, P.N., Daima, H.K., 2016. Rational engineering of physicochemical properties of nanomaterials for biomedical applications with nanotoxicological perspectives. Nano Converg. 3 https://doi.org/10.1186/s40580-016-0064-z.

Pal, I., Brahmkhatri, V.P., Bera, S., Bhattacharyya, D., Quirishi, Y., Bhunia, A., Atreya, H.S., 2016. Enhanced stability and activity of an antimicrobial peptide in conjugation with silver nanoparticle. J. Colloid Interface Sci. 483, 385–393. https://doi.org/10.1016/j.jcis.2016.08.043.

Pathak, S.D., Ng, L., Wyman, B., Fogarasi, S., Racki, S., Coelund, J., Sparks, B., Chalana, V., 2003. Quantitative image analysis: software systems in drug development trials. Drug Discov. Today 8 (10), 451–458. https://doi.org/10.1016/s1359-6446(03)02698-9.

Pei, Z., Sun, Q., Sun, X., Wang, Y., Zhao, P., 2015. Preparation and characterization of silver nanoparticles on silk fibroin/carboxymethylchitosan composite sponge as anti-bacterial wound dressing. Biomed. Mater. Eng. 26 (Suppl 1), S111–118. https://doi.org/10.3233/BME-151296.

Petros, R.A., DeSimone, J.M., 2010. Strategies in the design of nanoparticles for therapeutic applications. Nat. Rev. Drug Discov. 9 (8), 615–627. https://doi.org/10.1038/nrd2591.

Sahani, D., Saini, S., Fatuga, G.A., Halpern, E.F., Lanser, M.E., Zimmerman, J.B., Fischman, A.J., 2000. Quantitative measurements of medical images for pharmaceutical clinical trials: comparison between on-site and off-site assessments. AJR Am. J. Roentgenol. 174 (4), 1159–1162. https://doi.org/10.2214/ajr.174.4.1741159.

Scholz, M.-S., Blanchfield, J.P., Bloom, L.D., Coburn, B.H., Elkington, M., Fuller, J.D., Gilbert, M.E., Muflahi, S.A., Pernice, M.F., Rae, S.I., Trevarthen, J.A., White, S.C., Weaver, P.M., Bond, I.P., 2011. The use of composite materials in modern orthopaedic medicine and prosthetic devices: a review. Compos. Sci. Technol. 71 (16), 1791–1803. https://doi.org/10.1016/j.compscitech.2011.08.017.

Shao, Y., Wu, C., Wu, T., Yuan, C., Chen, S., Ding, T., Ye, X., Hu, Y., 2018. Green synthesis of sodium alginate-silver nanoparticles and their antibacterial activity. Int. J. Biol. Macromol. 111, 1281–1292. https://doi.org/10.1016/j.ijbiomac.2018.01.012.

Sharma, S., Sanpui, P., Chattopadhyay, A., Ghosh, S.S., 2012. Fabrication of antibacterial silver nanoparticle—sodium alginate–chitosan composite films. RSC Adv. 2 (13), 5837–5843. https://doi.org/10.1039/C2RA00006G.

Slater, T.J.A., Lewis, E.A., Haigh, S.J., 2016. Energy dispersive X-ray tomography for 3D elemental mapping of individual nanoparticles. J. Visual. Exp. JoVE 113. https://doi.org/10.3791/52815.

Spencer, J.A., Gao, Z., Moore, T., Buhse, L.F., Taday, P.F., Newnham, D.A., Shen, Y., Portieri, A., Husain, A., 2008. Delayed release tablet dissolution related to coating thickness by terahertz pulsed image mapping. J. Pharm. Sci. 97 (4), 1543–1550. https://doi.org/10.1002/jps.21051.

Takara, K., Hatakeyama, H., Ohga, N., Hida, K., Harashima, H., 2010. Design of a dual-ligand system using a specific ligand and cell penetrating peptide, resulting in a synergistic effect on selectivity and cellular uptake. Int. J. Pharm. 396 (1–2), 143–148. https://doi.org/10.1016/j.ijpharm.2010.05.002.

Tao, A., Sinsermsuksakul, P., Yang, P., 2006. Polyhedral silver nanocrystals with distinct scattering signatures. Angew. Chemie Int. Ed. 45 (28), 4597–4601. https://doi.org/10.1002/anie.200601277.

Tavakoli, A., Sohrabi, M., Kargari, A., 2007. A review of methods for synthesis of nanostructured metals with emphasis on iron compounds. Chem. Pap. 61 (3), 151–170. https://doi.org/10.2478/s11696-007-0014-7.

Thakkar, K.N., Mhatre, S.S., Parikh, R.Y., 2010. Biological synthesis of metallic nanoparticles. Nanomed. Nanotechnol. Biol. Med. 6 (2), 257–262. https://doi.org/10.1016/j.nano.2009.07.002.

Velusamy, P., Su, C.-H., Venkat Kumar, G., Adhikary, S., Pandian, K., Gopinath, S.C.B., Chen, Y., Anbu, P., 2016. Biopolymers regulate silver nanoparticle under microwave irradiation for effective antibacterial and antibiofilm activities. PLoS One 11 (6), e0157612. https://doi.org/10.1371/journal.pone.0157612.

Wiley, B., Sun, Y., Mayers, B., Xia, Y., 2005. Shape-controlled synthesis of metal nanostructures: the case of silver. Chem. Eur. J. 11 (2), 454–463. https://doi.org/10.1002/chem.200400927.

Wu, Y.S., van Vliet, L.J., Frijlink, H.W., van der Voort Maarschalk, K., 2007. Pore size distribution in tablets measured with a morphological sieve. Int. J. Pharm. 342 (1–2), 176–183. https://doi.org/10.1016/j.ijpharm.2007.05.011.

Yang, J., Zheng, H., Han, S., Jiang, Z., Chen, X., 2014. The synthesis of nano-silver/sodium alginate composites and their antibacterial properties. RSC Adv. 5 (4), 2378–2382. https://doi.org/10.1039/C4RA12836B.

Yuan, J., Wang, D., Cheriyadat, A.M., 2015. Factorization-based texture segmentation. Ieee Trans. Image Process. 24 (11), 3488–3497. https://doi.org/10.1109/TIP.2015.2446948.

Zaitoun, N.M., Aqel, M.J., 2015. Survey on image segmentation techniques. Procedia Comput. Sci. 65, 797–806. https://doi.org/10.1016/j.procs.2015.09.027.

Zeitler, J.A., Shen, Y., Baker, C., Taday, P.F., Pepper, M., Rades, T., 2007. Analysis of coating structures and interfaces in solid oral dosage forms by three dimensional terahertz pulsed imaging. J. Pharm. Sci. 96 (2), 330–340. https://doi.org/10.1002/jps.20789.

Zhang, C., Liu, L.-H., Qiu, W.-X., Zhang, Y.-H., Song, W., Zhang, L., Wang, S.-B., Zhang, X.-Z., 2018. A transformable chimeric peptide for cell encapsulation to overcome multidrug resistance. Small 14 (11), e1703321. https://doi.org/10.1002/smll.201703321.